The Astrophysical Journal, 728:108 (10pp), 2011 February 20 doi:10.1088/0004-637X/728/2/108

VARYING ALPHA FROM *N*-BODY SIMULATIONS

Baojiu Li[1,2], David F. Mota[3], and John D. Barrow[1]
[1] DAMTP, Centre for Mathematical Sciences, University of Cambridge, Wilberforce Road, Cambridge CB3 0WA, UK;
b.li@damtp.cam.ac.uk, j.d.barrow@damtp.cam.ac.uk
[2] Kavli Institute for Cosmology Cambridge, Madingley Road, Cambridge CB3 0HA, UK
[3] Institute of Theoretical Astrophysics, University of Oslo, 0315 Oslo, Norway; d.f.mota@astro.uio.no
Received 2010 September 4; accepted 2010 December 13; published 2011 January 26

ABSTRACT

We have studied the Bekenstein–Sandvik–Barrow–Magueijo (BSBM) model for the spatial and temporal variations of the fine structure constant, α, with the aid of full *N*-body simulations that explicitly and self-consistently solve for the scalar field driving the α-evolution. We focus on the scalar field (or equivalently α) inside the dark matter halos and find that the profile of the scalar field is essentially independent of the BSBM model parameter. This means that given the density profile of an isolated halo and the background value of the scalar field, we can accurately determine the scalar-field perturbation in that halo. We also derive an analytic expression for the scalar-field perturbation using the Navarro–Frenk–White halo profile and show that it agrees well with numerical results, at least for isolated halos; for non-isolated halos, this prediction differs from numerical result by a (nearly) constant offset, which depends on the environment of the halo.

Key words: cosmology: miscellaneous – dark matter – large-scale structure of universe – methods: numerical

Online-only material: color figures

1. INTRODUCTION

During the past 10 years, interest has continued in the search for possible time and space variation of fundamental constants of nature. This interest was stimulated by observations of quasar absorption spectra that are consistent with a slow increase of the fine structure "constant," α, over cosmological timescale (Webb et al. 1999, 2001). Experimental and observational efforts to constrain the level of any possible time variation in fundamental constants have a history that pre-dates modern theories about how they might vary (for reviews see Barrow 2002, 2005, Uzan 2003, 2010, and Olive & Qian 2004).

Until quite recently, all the observational studies found no evidence for any variations. However, data from a number of astronomical observations have provided evidence that at least two of these constants, the fine structure constant: $\alpha = e^2/\hbar c$ (where e is the electric charge of electron), and the electron–proton mass ratio: $\mu = m_e/m_p$ might have varied slightly over cosmological time. Using a data set of 128 KECK-HIRES quasar absorption systems at redshifts $0.5 < z < 3$, and a new many-multiplet (MM) analysis of the line separations between many pairs of atomic species possessing relativistic corrections to their fine structure, Webb et al. (1999, 2001) found the observed absorption spectra to be consistent with a shift in the value of the fine structure constant, α, between those redshifts and the present day, with $\Delta\alpha/\alpha \equiv \alpha(z) - \alpha(0)/\alpha(0) = (-0.57 \pm 0.10) \times 10^{-5}$. A smaller study of 23 VLT-UVES absorption systems between $0.4 \leqslant z \leqslant 2.3$ by Chand et al. (2004) and Siranand et al. (2004) initially found $\Delta\alpha/\alpha = (-0.6 \pm 0.6) \times 10^{-6}$ by using a version of the full MM analysis technique. However, the reanalysis of the same data set by Murphy et al. (2007, 2008) increased the uncertainties and suggested a revised figure of $\Delta\alpha/\alpha = (-0.64 \pm 0.36) \times 10^{-5}$ for the same data; see also the discussion in Murphy et al. (2007, 2008) and Siranand et al. (2008). These investigations relied on the statistical gain from large samples of quasar absorption spectra. Detailed analyses of sources of systematic error continue, particularly for the effects pointed out recently by Griest et al. (2010) and Whitmore et al. (2010), which have now been studied in detail by J. A. King et al. (2011, in preparation). Most recently, this observational programme has been extended to both hemispheres of the sky using KECK and VLT samples of 153 absorption systems by Webb et al. (2010) and finds evidence consistent with an increase in α in the northern sky but consistent with a slow decrease in α with time in the south. When combined these overlapping data sets are well fitted by a dipole with $\Delta\alpha/\alpha_0 = (1.10 \pm 0.25) \times 10^{-6}\, r \cos\theta$, at measurement position $\underline{r}$ (relative to Earth at $\underline{r} = 0$), where θ is the angle between the measurement and the axis of the dipole. These observations will be subject to further scrutiny by observers. In the meantime, they suggest that we should develop an understanding of the spatial as well as the temporal consequences of varying constants.

Theoretically, a variation in α could be due to a light scalar field, as described by a model like that of Bekenstein, Sandvik, Barrow, and Magueijo (BSBM from here on; Bekenstein 1982; Sandvik et al. 2002; Magueijo et al. 2002). In the BSBM model, a scalar field φ couples only to the electromagnetic part of the matter action, which contributes little to the total energy–momentum tensor throughout the cosmic history and so drives a very slow time variation of α as constrained by observational data. This model has been subsequently investigated in great details in terms of the predicted time evolution of α.

On the other hand, it is well known that a scalar field could cluster and be inhomogeneous on large scales. As the value of the scalar field is directly related to α, one expects inhomogeneities in α in scenarios where variations in α are induced by a massive scalar field with a mass (m_φ). In particular, one would expect variations in α on cosmological scales to differ from those on scales below the field's Jeans length, which is $O(1/m_\varphi)$. Some detailed analysis of the global–local coupling of variations in constants can be found in Clifton et al. (2005), Mota & Barrow (2004a, 2004b), Shaw & Barrow (2006a, 2006b, 2006c), and Olive & Pospelov (2008), but these studies are mostly semi-analytical or have made simplifying approximations about the value of the scalar field.

In this paper, we will study the BSBM model for the spatial and temporal variations of the fine structure constant α, with the aid of full N-body simulations that explicitly and self-consistently solve for the scalar field driving α-evolution. We focus on the trend of the scalar field (or equivalently, α) inside the dark matter halos and find that the profile of the scalar-field fluctuation is essentially independent of the BSBM model parameter. This means that given the density profile of an isolated halo and the background value of the scalar field, we can accurately determine the scalar-field perturbation in that halo. We also derive an analytic expression for the scalar-field perturbation using the Navarro–Frenk–White (NFW) halo profile and show that it agrees well with numerical results, at least for isolated halos. For non-isolated halos this exact prediction differs from numerical result by a (nearly) constant offset, depending on the environment of this halo.

A brief outline of the remaining of this paper is as follows. In Section 2, we list the minimal set of necessary equations to understand the physics and briefly describe our algorithm; Section 3 displays the main numerical results, and we then discuss and conclude in Section 4.

2. EQUATIONS AND ANALYSIS

This section lists the equations which will be used in the N-body simulations for the BSBM varying-α model (Barrow & Mota 2003; Barrow et al. 2002a, 2002b; Sandvik et al. 2002; Mota & Barrow 2004a, 2004b).

2.1. The Basic Equations

The Lagrangian density for the BSBM model could be written as

$$\mathcal{L} = \frac{1}{2}\left[\frac{R}{\kappa} - \nabla^a\varphi\nabla_a\varphi\right] - \mathcal{L}_m - e^{-2\sqrt{\kappa}\varphi}\mathcal{L}_{\rm EM} - \mathcal{L}_r, \quad (1)$$

where R is the Ricci scalar, $\kappa = 8\pi G$ with G being the gravitational constant, φ is the scalar field; $\mathcal{L}_m$, $\mathcal{L}_{\rm EM}$, and $\mathcal{L}_r$ represent respectively the Lagrangian densities for dust, electromagnetic field (including photons), and other radiation (such as neutrinos). The coupling function between the scalar field and the electromagnetic field in the BSBM model is $e^{-2\sqrt{\kappa}\varphi}$, where $\sqrt{\kappa}$ is added so that $\sqrt{\kappa}\varphi \equiv \psi$ is dimensionless. In the simplest version of the model, there is no potential for the scalar field.

The dust Lagrangian for a point particle with mass m_0 is

$$\mathcal{L}_m(\mathbf{y}) = -\frac{m_0}{\sqrt{-g}}\delta(\mathbf{y}-\mathbf{x}_0)\sqrt{g_{ab}\dot{x}_0^a\dot{x}_0^b}, \quad (2)$$

where $\mathbf{y}$ is the general coordinate and $\mathbf{x}_0$ is the coordinate of the center of the particle. From this equation, we derive the corresponding energy–momentum tensor

$$T_m^{ab} = \frac{m_0}{\sqrt{-g}}\delta(\mathbf{y}-\mathbf{x}_0)\dot{x}_0^a\dot{x}_0^b. \quad (3)$$

Also, because $g_{ab}\dot{x}_0^a\dot{x}_0^b \equiv g_{ab}u^au^b = 1$, in which u^a is the 4-velocity of the dark matter particle centered at x_0, the Lagrangian can be rewritten as

$$\mathcal{L}_m(\mathbf{y}) = -\frac{m_0}{\sqrt{-g}}\delta(\mathbf{y}-\mathbf{x}_0). \quad (4)$$

This result will be used below.

Equation (3) is just the energy–momentum tensor for a single matter particle. For a fluid consisting of many particles, the energy–momentum tensor will be

$$T_m^{ab} = \frac{1}{\mathcal{V}}\int_{\mathcal{V}} d^4y\sqrt{-g}\frac{m_0}{\sqrt{-g}}\delta(y-x_0)\dot{x}_0^a\dot{x}_0^b = \rho_{\rm CDM}u^au^b, \quad (5)$$

where $\mathcal{V}$ denotes a volume that is microscopically large but macroscopically small, and we have extended the three-dimensional δ function to a four-dimensional one by adding a time component. Here, u^a is the averaged 4-velocity of the matter fluid.

Using

$$T^{ab} = -\frac{2}{\sqrt{-g}}\frac{\delta(\sqrt{-g}\mathcal{L})}{\delta g_{ab}}, \quad (6)$$

it is straightforward to show that the energy–momentum tensor for the scalar field is

$$T^{\varphi ab} = \nabla^a\varphi\nabla^b\varphi - \tfrac{1}{2}g^{ab}\nabla_c\varphi\nabla^c\varphi. \quad (7)$$

Therefore, the total energy–momentum tensor is

$$T_{ab} = \nabla_a\varphi\nabla_b\varphi - \frac{1}{2}g_{ab}\nabla_c\varphi\nabla^c\varphi + T_{ab}^m + T_{ab}^r + e^{-2\sqrt{\kappa}\varphi}T_{ab}^{\rm EM}, \quad (8)$$

where $T_{ab}^m = \rho_m u_a u_b$, $T_{ab}^{\rm r}$ is the energy–momentum tensor for radiation fields except photons, and $T_{ab}^{\rm EM}$ for photons. The Einstein equations are

$$G_{ab} = \kappa T_{ab} \quad (9)$$

in which $G_{ab} = R_{ab} - \frac{1}{2}g_{ab}R$ is the Einstein tensor. Note that due to the extra coupling between the scalar field, φ, and the electromagnetic field, the energy–momentum tensors for either will no longer be separately conserved, but instead we have

$$\nabla_b T_{\rm EM}^{ab} = 2\sqrt{\kappa}\left(g^{ab}\mathcal{L}_{\rm EM} + T_{\rm EM}^{ab}\right)\nabla_b\varphi. \quad (10)$$

However, the total energy–momentum tensor is certainly conserved.

Meanwhile, the scalar-field equation of motion is

$$\Box\varphi = -2\sqrt{\kappa}e^{-2\sqrt{\kappa}\varphi}\mathcal{L}_{\rm EM}, \quad (11)$$

where $\Box \equiv \nabla^a\nabla_a$. This equation governs the time evolution and spatial configuration of the scalar field.

Equations (8)–(11) summarize all the physics needed for the following analysis. However, when making use of them we should also specify the form of the electromagnetic matter. For example, if it is a pure electromagnetic field (photons), then we have $\mathcal{L}_{\rm EM} = \frac{1}{2}(E^2 - B^2) = 0$ in which E and B stand for the electric and magnetic fields, respectively. Thus, from the time component of Equation (10) we obtain the (background) evolution equation for photon density as

$$\dot{\rho}_r + 4H\rho_r = 2\dot{\psi}\rho_r, \quad (12)$$

where H is the Hubble expansion rate and remember that $\psi = \sqrt{\kappa}\varphi$.

It then seems that, by the same reason, the right-hand side of Equation (11) also vanishes, leaving the scalar field

unsourced. This may not be true however, as non-relativistic matter could also contribute to $\mathcal{L}_{\rm EM}$ and thus $T^{\rm EM}_{ab}$. For example, in baryonic matter $\mathcal{L}_{\rm EM} \approx E^2/2$, and for neutrons and protons this electromagnetic contribution to the total mass can be of order 10^{-4}; in superconducting cosmic strings $\mathcal{L}_{\rm EM} \approx -B^2/2$, where $\rho_{\rm EM} \approx B^2/2$ so that $|\mathcal{L}_{\rm EM}/\rho_{\rm EM}| \sim 1$. In the BSBM model, in order to simplify the situation, it is assumed that $\mathcal{L}_{\rm EM}/\rho_m = \zeta$, where ζ is a constant with a modulus between 0 and ≈ 1, either positive or negative, and ρ_m is the density for non-relativistic matter.

Thus, the scalar-field equation gets sourced by a term proportional to ζ:

$$\Box\varphi = -2\sqrt{\kappa}\zeta e^{-2\sqrt{\kappa}\varphi}\rho_m. \tag{13}$$

Since the part of $\mathcal{L}_{\rm EM}$ that affects the scalar field is a constituent of the non-relativistic matter and is presumably moving with the matter particles, we could combine Equation (10) and the conservation equation for the dust matter (no including electromagnetic contribution) to write a new conservation equation for the particle:

$$\nabla_b T^{ab}_{m+\rm EM} = 2\sqrt{\kappa}\left(g^{ab}\mathcal{L}_{\rm EM} + T^{ab}_{\rm EM}\right)\nabla_b\varphi. \tag{14}$$

Although we have assumed above that $\mathcal{L}_{\rm EM} = \zeta\rho_m$, we still lack knowledge about $T^{ab}_{\rm EM}$, whose relation to $\mathcal{L}_{\rm EM}$ could be complicated. Here, for simplicity, we assume that $T^{ab}_{\rm EM} = -\zeta\rho_m u^a u^b$. Then it is easy to find that the time component of this equation reads

$$\dot{\rho}_{m+\rm EM} + 3H\rho_{m+\rm EM} = 0, \tag{15}$$

while the ith spatial component of it gives the following (modified) geodesic equation:

$$\ddot{x}^i_0 + \Gamma^i_{ab}\dot{x}^a_0\dot{x}^b_0 = 2\zeta\sqrt{\kappa}(g^{ib} - u^i u^b)\nabla_b\varphi, \tag{16}$$

where x_0 is the coordinate of the center of a particle, and the right-hand side represents a fifth force on the particle (Li & Zhao 2009, 2010). The assumption $T^{ab}_{\rm EM} = -\zeta\rho_m u^a u^b$ might seem unappealing, but as we shall see below, because $|\zeta| \ll 1$, the fifth force is much weaker than gravity and thus has negligible effects in the clustering of matter in any case; ultimately, it is only the BSBM assumption $\mathcal{L}_{\rm EM} = \zeta\rho_m$ that is important in theoretical predictions of the spatial and temporal variations of α, given that $\alpha = e^{2\psi}\frac{e_0^2}{c\hbar}$, where e_0 is the present-day value for e.

2.2. Analytical Approximation

The scalar-field equation of motion, which controls the dynamics of the scalar field φ, is generally complicated, because it depends nonlinearly on φ, which both evolves in time and fluctuates in space. Fortunately, for the majority of applications the scalar-field potential and coupling function are not nonlinear enough to give the scalar field a very heavy mass so as to make it fluctuate strongly. The nice thing about this is that in certain places of the equations one may then forget the scalar-field perturbation and simplify these equations accordingly. In Li & Barrow (2011), for example, it is shown that such a simplification is a very good approximation (see, however, Li & Zhao 2009, 2010 for an opposite extreme for which the scalar-field potential is very nonlinear so that such simplification does not work).

In the BSBM model, there is no scalar-field potential and the coupling function is close to linear if $\sqrt{\kappa}|\varphi| \ll 1$ (which is the case for parameter space that we are interested in; Barrow et al. 2002a). We therefore expect the fluctuation of φ to be very weak and assume that $\sqrt{\kappa}|\delta\varphi| \ll \sqrt{\kappa}|\varphi| \ll 1$ (which we shall confirm below using numerical simulations). Under such an assumption the Poisson equation could be written as

$$\begin{aligned}\nabla^2_{\mathbf{x}}\Phi &= 4\pi G a^3\rho_m[1 + \zeta e^{-2\sqrt{\kappa}(\bar{\varphi}+\delta\varphi)}] - 4\pi G a^3\bar{\rho}_m[1 + \zeta e^{-2\sqrt{\kappa}\bar{\varphi}}] \\ &\approx 4\pi G a^3(\rho_m - \bar{\rho}_m),\end{aligned} \tag{17}$$

where $\bar{\varphi}$ is the background value of φ and $\delta\varphi$is its perturbation; ρ_m, $\bar{\rho}_m$ are respectively the local and background matter density; Φ is the gravitational potential and a is the cosmic scale factor; $\nabla_{\mathbf{x}}$ is the derivative with respect to the comoving coordinate $\mathbf{x}$. To obtain Equation (17), we have used the fact that in the BSBM model $|\zeta e^{-2\bar{\varphi}}| \ll 1$. Note that Equation (17) clearly indicates that the gravitational potential is essentially not influenced by the scalar field φ.

For the scalar-field equation of motion Equation (13), because the background part (which has no spatial dependence) can be solved easily, we subtract that from the full equation to obtain an equation of motion for $\delta\varphi$ only (remember that $\varphi = \bar{\varphi} + \delta\varphi$). Furthermore, we drop the time derivative terms of $\delta\varphi$, as they are small compared with the spatial gradients (i.e., work in the quasi-static limit). The final equation for $\delta\varphi$ then becomes

$$\begin{aligned}\nabla^2_{\mathbf{x}}(a\sqrt{\kappa}\delta\varphi) &= 2\zeta\kappa[\rho_m e^{-2\sqrt{\kappa}(\bar{\varphi}+\delta\varphi)} - \bar{\rho}_m e^{-2\sqrt{\kappa}\bar{\varphi}}]a^3 \\ &\approx 16\pi G a^3\zeta(\rho_m - \bar{\rho}_m),\end{aligned} \tag{18}$$

where we have used $\kappa = 8\pi G$ and $\sqrt{\kappa}|\delta\varphi| \ll \sqrt{\kappa}|\varphi| \ll 1$.

Comparing Equations (17) and (18), it is evident that the source terms are the same up to a constant coefficient 4ζ. Consequently, we shall have

$$a\sqrt{\kappa}\delta\varphi(\mathbf{x}) \approx 4\zeta\Phi(\mathbf{x}). \tag{19}$$

Note that this equation, together with the geodesic equation (16), implies that the magnitude of the fifth force (force due to exchange of scalar-field quanta between particles) $|\mathbf{f}|$ satisfies

$$|\mathbf{f}| \sim \zeta|\vec{\nabla}(a\sqrt{\kappa}\delta\varphi)| \sim 4\zeta^2|\vec{\nabla}\Phi|. \tag{20}$$

Therefore, the ratio between the magnitudes of the fifth force and gravity is of order $\zeta^2 \lesssim 10^{-12}$ to $10^{-8} \ll 1$. This implies that the fifth force cannot significantly influence the structure formation.

3. SIMULATIONS AND RESULTS

3.1. φ Perturbation Versus Gravitational Potential

To study in details the behavior of the scalar field and hence the fine structure constant α in the BSBM model, we have performed N-body simulations for four different models, with $\zeta = \pm 2 \times 10^{-6}$ and $\pm 5 \times 10^{-6}$, respectively. The physical parameters that we adopt in all simulations are as follows: the present-day dark-energy fractional-energy density $\Omega_{\rm DE} = 0.743$ and $\Omega_m = \Omega_{\rm CDM} + \Omega_{\rm B} = 0.257$, $H_0 = 71.9\,{\rm km\,s^{-1}\,Mpc^{-1}}$, $n_s = 0.963$, and $\sigma_8 = 0.761$. These are in accordance with the concordance cosmological model preferred by current data sets. Our simulation box has a size of $64\,h^{-1}$ Mpc, in which $h = H_0/(100\,{\rm km\,s^{-1}\,Mpc^{-1}})$. In all of those simulations, the mass resolution is $1.114 \times 10^9\,h^{-1}\,M_\odot$; the particle number is 256^3; the domain grid (i.e., the coarsest grid which covers the whole simulation box) has 128^3 equal-sized cubic cells; and the

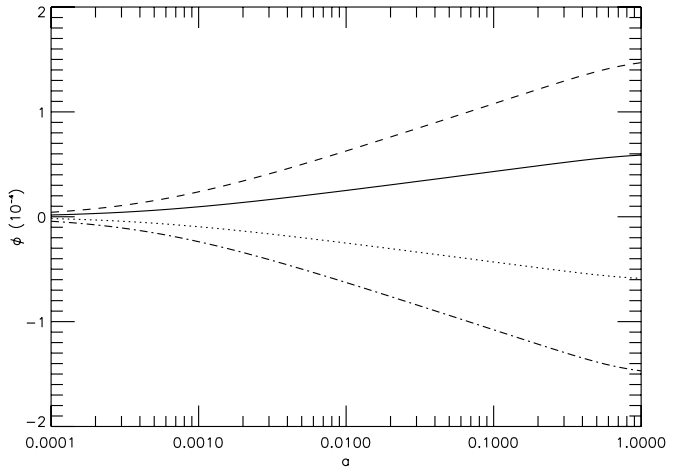

Figure 1. Time evolution of $\bar{\varphi}$ for the four models considered in this work, with $\zeta = -2 \times 10^{-6}$ (solid curve), 2×10^{-6} (dotted curve), -5×10^{-6} (dashed curve), and 5×10^{-6} (dash-dotted curve), respectively. The horizontal axis is the cosmic scale factor $a(t)$ and the vertical axis plots $\sqrt{\kappa}\bar{\varphi}$ in unit of 10^{-4}.

finest refined grids have 16,384 cells on each side, corresponding to a force resolution of $\sim 12\,h^{-1}$ kpc. Detailed description about the N-body simulation technique and code for the (coupled) scalar-field models could be found in Li & Zhao (2009, 2010) and will not be presented here.

Because the BSBM model (with the parameter ζ constrained by data) involves a very weak coupling between matter and the scalar field φ, the presence of the latter and its coupling have negligible influences on the background (ΛCDM) cosmology, although the opposite is not true since there is no scalar-field potential and thus the dynamics of φ is controlled entirely by the coupling. In our simulations, we compute the full background cosmology and evolution of φ on a predefined time grid using the MAPLE mathematical software, and interpolate to obtain the corresponding quantities which are needed in N-body simulations. Details of this procedure can be found in Appendix C of Li & Barrow (2011), and Figure 1 shows the background evolution of $\sqrt{\kappa}\varphi$ for the four models considered here. Obviously the condition $\sqrt{\kappa}\bar{\varphi} \ll 1$ is satisfied, justifying the approximation we used above to derive Equation (19).

One nice thing about the BSBM model is its simplicity, and it turns out that the background evolution of φ (and thus α) in different cosmic epochs can be well described by some analytical formulae (Barrow et al. 2002a). Therefore, in the present study, we shall mainly focus on the spatial variation of φ and α (especially in virialized halos).

As mentioned above, because there is no potential for the scalar field φ and because $\sqrt{\kappa}\varphi \ll 1$ for our choices of ζ, the scalar-field equation of motion (in the quasi-static limit) for $\delta\varphi$ and the Poisson equation share the same source up to a constant coefficient, and therefore we expect $a\delta\varphi \propto \Phi$ across the whole space. This is what we have found in Li & Barrow (2011) for a different coupled scalar-field model where the scalar-field potential is negligible. Indeed, this could serve as a test of the scalar-field solver in our N-body simulation code.

To check that our code does recover the analytical approximation, we have plotted in Figure 2 the comparison of the scalar-field perturbation $a\sqrt{\kappa}\delta\varphi$ and gravitational potential Φ from a slice of the simulation box. As indicated by this figure, the agreement between the numerical results (green dots) and analytical approximation (black solid line) is remarkably good, implying that the numerical code works well. Therefore to a high precision we can assume that $a\sqrt{\kappa}\delta\varphi \propto \Phi$ everywhere, a fact that will be used below to obtain an analytical expression of $\delta\varphi$ in dark matter halos.

3.2. Spatial Variation of φ in Halos

In the standard picture, the galaxies where observers live generally locate inside the dark matter halos, which to the simplest approximation are just spherical clusters of matter with a universal NFW (Navarro et al. 1996) density profile.

We are certainly interested in the (possible) variation of α inside the halo in which we reside. For example, there has been a great deal of analytical work on how significantly the local value of α could deviate from its cosmological counterpart (Mota & Barrow 2004a, 2004b; Jacobson 1999; Wetterich 2003; Shaw & Barrow 2006a, 2006b, 2006c). Also, if the spatial variation of α is strong enough, then it might have an impact on our observation of the spectra for the stars from our Galaxy and other galaxies.

From our simulation output, it is easy to identify the dark matter halos (Knebe & Gibson 2004; Li & Barrow 2011). Now what we want to do here is to measure the quantity $\sqrt{\kappa}\delta\varphi$ as a function of distance R to the halo centers, assuming that the halos are exactly spherical. For this we have recorded the value for $\sqrt{\kappa}\delta\varphi$ at the position of each particle, and then presumably we could divide each halo into a number of spherical shells, determine the radius of each shell and compute the average value of $\sqrt{\kappa}\delta\varphi$ in the shells. However, there is some subtlety in the computation of the averaged $\sqrt{\kappa}\delta\varphi$.

The problem is that, since we have only recorded the information for $\sqrt{\kappa}\delta\varphi$ at the positions of the particles, we do not have fair sampling points. Because $\sqrt{\kappa}\delta\varphi$ tends to be different in regions of different particle number densities, the high-density regions will be oversampled and low-density regions undersampled, resulting in a bias as we are trying to determine the spatially averaged, rather than the particle-averaged, value of $\sqrt{\kappa}\delta\varphi$. To test how large the bias could be, we use an approximation as follows: first, we divide each spherical shell into N equal-sized volumes which are small enough so that the particle number density does not change much inside each of them, then we compute the particle average of $\sqrt{\kappa}\delta\varphi$ in each of these volumes, call it $\langle\sqrt{\kappa}\delta\varphi\rangle_i$ for $i = 1, \ldots, N$, then the spatial (volume) average of $\sqrt{\kappa}\delta\varphi$ is given by

$$\langle\sqrt{\kappa}\delta\varphi\rangle_{\rm Vol} \approx \frac{1}{N}\sum_{i=1}^{N}\langle\sqrt{\kappa}\delta\varphi\rangle_i. \tag{21}$$

More precise treatments of the volume average could be obtained by using space tessellations, such as Delaunay triangulation, but this is too technical and thus beyond the scope of this work. Anyway, using our approximation Equation (21), we find that the bias caused by using particle-number average is at most 1%–2%, which is not unacceptable considering that the sphericity of halos is already an approximation.

Figure 3 shows the profile of $\sqrt{\kappa}\delta\varphi$ inside the dark matter halos. Instead of plotting this halo by halo, we have selected the 80 most massive halos from our simulation box, and divided them into six bins with $M/(10^{14}\,M_\odot) \in [2.0, \infty)$, [1.0, 2.0], [0.6, 1.0], [0.3, 0.6], [0.2, 0.3], and [0.1, 0.2]. Then, we compute the averaged profile of $\sqrt{\kappa}\delta\varphi$ in each of the six bins (the six curves in Figure 3). As expected, the larger the halo is, the deeper the gravitational potential is and, because $a\sqrt{\kappa}\delta\varphi \approx \Phi$, the larger $|\sqrt{\kappa}\varphi|$ is. Meanwhile, going from the

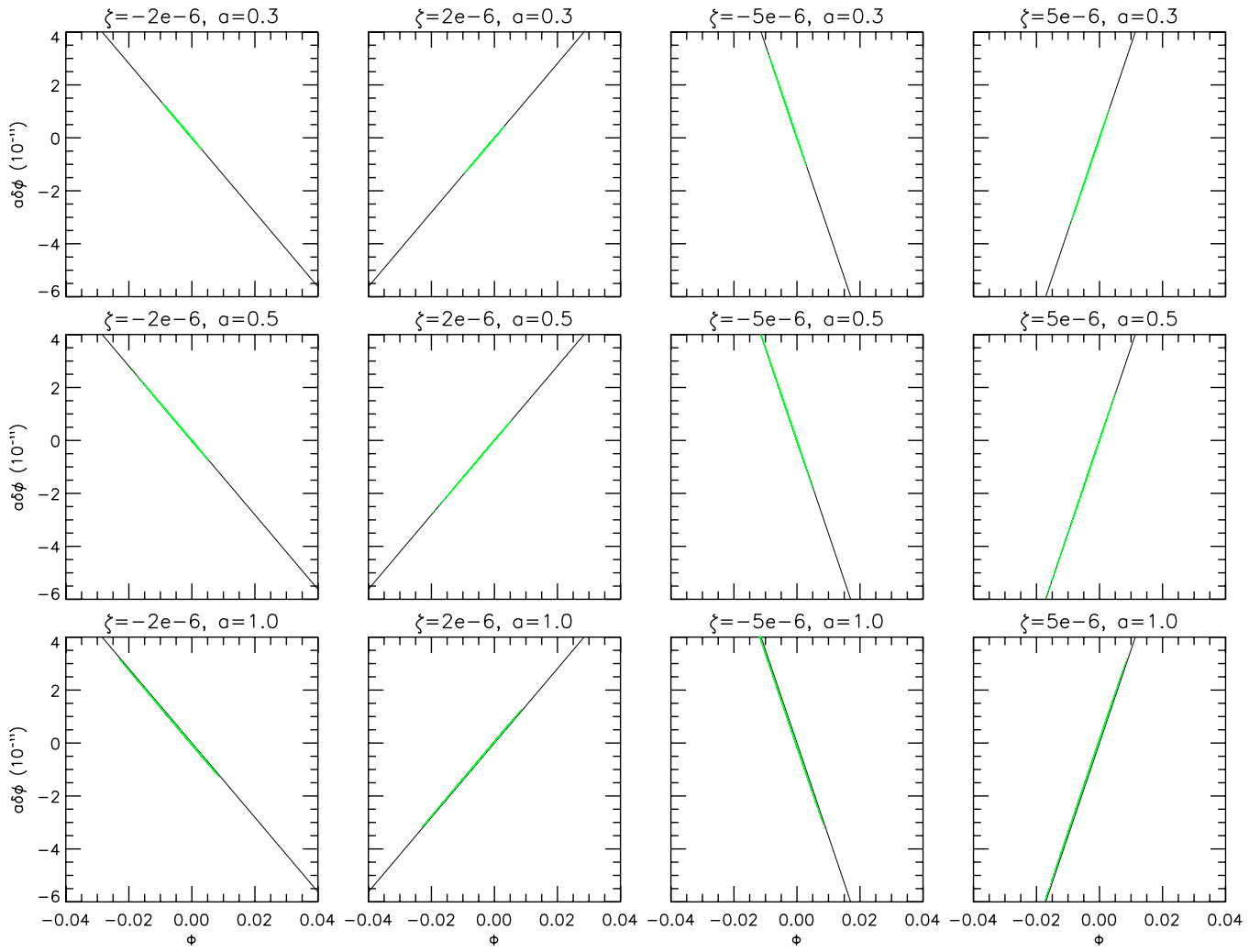

Figure 2. Scatter plot of the scalar-field perturbation, $a\sqrt{\kappa}\delta\varphi$ (vertical axis, in unit of 10^{-11}) vs. gravitational potential Φ (horizontal axis) in code units. The black solid line is the analytical approximation $a\delta\varphi \propto \Phi$; each green dot represents the corresponding result measured in a cell from a particular slice that is randomly selected from the simulation box. The columns are for four models with $\zeta = \pm 2, \pm 5 \times 10^{-6}$ as shown above each panel, and the rows are for three different output times $a = 0.3, 0.5, 1.0$, also shown above each panel. Note that the slopes for the solid lines differ because of the different values of ζ.

(A color version of this figure is available in the online journal.)

halo center outward one finds that $|\sqrt{\kappa}\varphi|$ gradually decreases (toward 0), which makes sense because $\sqrt{\kappa}\delta\varphi \to 0$ as $R \to \infty$. Finally, we also note that the value of $\sqrt{\kappa}\delta\varphi$ depends sensitively on ζ and $|\sqrt{\kappa}\delta\varphi|$ increases with $|\zeta|$.

Figure 3 also shows that for our choices of ζ the value of $|\sqrt{\kappa}\delta\varphi|$ is typically of order 10^{-10} to 10^{-9}, which is quite small but gives us no idea how large the fluctuation in φ is. For the latter, we have instead plotted the profile of the quantity $\delta\varphi/\varphi$ inside the 80 halos distributed in six bins. Interestingly, unlike $\delta\varphi$, the quantity $\delta\varphi/\varphi$ does not depend on the sign of ζ, and indeed it almost does not depend on the magnitude of ζ either. This, together with the facts that (1) $a\sqrt{\kappa}\delta\varphi(R, a) \propto \Phi(R, a)$, and (2) the presence of the scalar field and its coupling to matter have negligible effect in the structure formation (so that the halo density profile remains NFW), indicates that the fluctuation of φ in the BSBM model only depends on the non-BSBM physical parameters, and once we have solved the background value of φ, we might gain some knowledge of the $\sqrt{\kappa}\delta\varphi$ profile without solving it explicitly (see below for further details).

Because the BSBM model is designed for the variation of α, we are also interested in how large this variation, $\delta\alpha/\alpha$, is. Because $\alpha \propto e^{2\sqrt{\kappa}\varphi}$, we have $\delta\alpha/\alpha = 2\sqrt{\kappa}\delta\varphi$. From Figure 3, we clearly see that this is of order 10^{-10} to 10^{-9} across galaxy clusters, where the exact value depends on both the size of the halo and the model parameters. Levshakov et al. (2010c) have given an upper limit of the spatial variation of α in Milky Way, $|\delta\alpha/\alpha| < 2 \times 10^{-7}$, and the BSBM prediction is well within this bound. Levshakov et al. (2010a, 2010b) also found that in the Milky Way the spatial variation of μ is $\delta\mu/\mu = 26 \pm 1(\text{stat}) \pm 3(\text{sys}) \times 10^{-9}$, which is comparable to the spatial variation of α predicted by the BSBM model.

Now, given that the NFW profile for dark matter halos is (expected to be) preserved in the varying-α simulations, we wonder whether it is possible to derive some analytical (approximate) formula for the profile of $\sqrt{\kappa}\varphi$. For this let us recall that the NFW profile is expressed as

$$\frac{\rho(r)}{\rho_c} = \frac{\beta}{\frac{r}{R_s}\left(1 + \frac{r}{R_s}\right)^2}, \tag{22}$$

where ρ_c is the critical density for matter, β is a dimensionless fitting parameter, and R_s is a second fitting parameter with length dimension. β and R_s are generally different for different halos and should be fitted for individual halos.

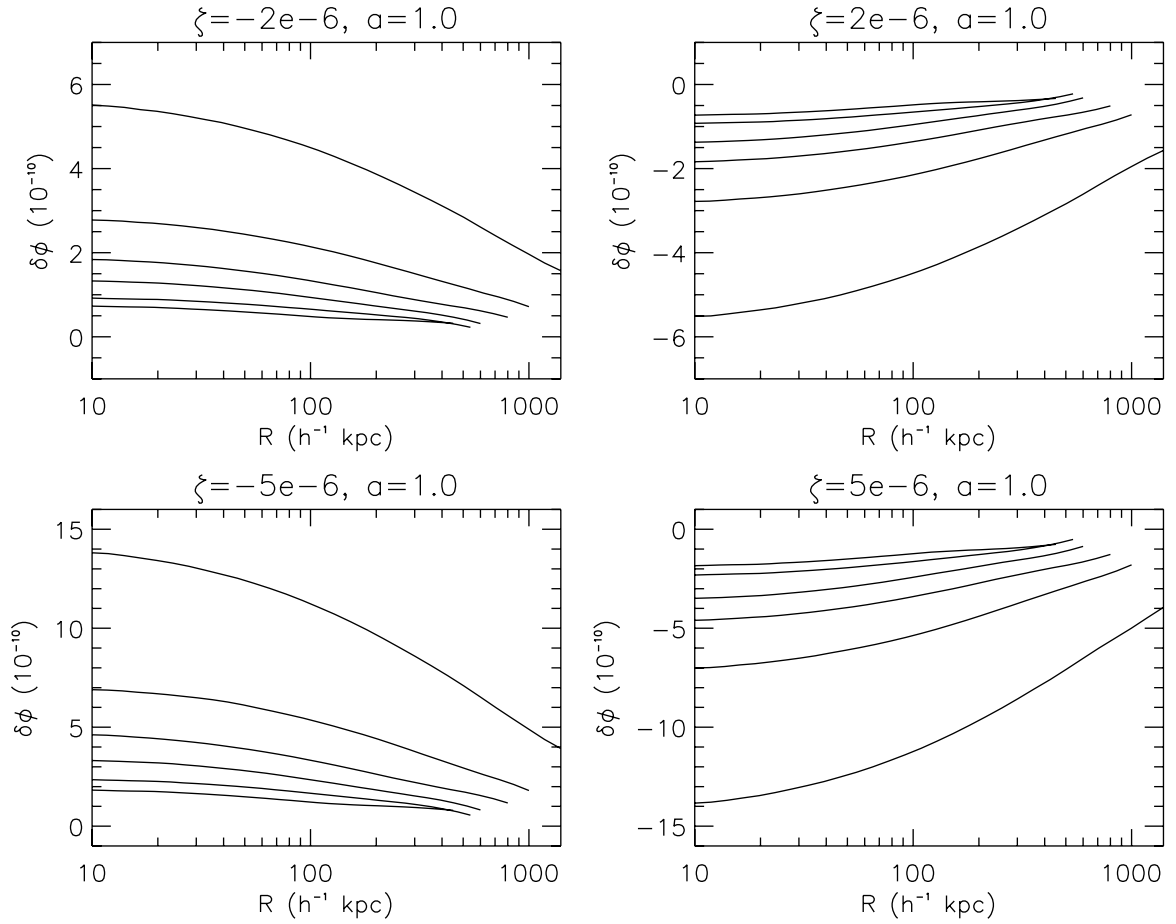

Figure 3. Profile of $a\sqrt{\kappa}\delta\varphi$ inside the halos for the four models with $\zeta = \pm 2, \pm 5 \times 10^{-6}$ as indicated at the top of each panel. We have considered the 80 most massive halos from the simulation box and divided them into six bins with $M/\left(10^{14} M_{\odot}\right) \in [2.0, \infty)$, [1.0, 2.0], [0.6, 1.0], [0.3, 0.6], [0.2, 0.3], and [0.1, 0.2], respectively. Each curve represents the averaged profile of $a\sqrt{\kappa}\delta\varphi$ for one bin (the more massive bins always correspond to larger, either positive or negative—depending on the sign of ζ—deviations from zero). All results are for output time $a = 1.0$ (today). The horizontal axis is the distance R to the halo center, in units of h^{-1} kpc and the vertical axis is $a\sqrt{\kappa}\delta\varphi$ in units of 10^{-10}.

We have checked the halos in our analysis and found that the majority of them are indeed very well described by Equation (22), confirming our earlier argument that the coupled scalar-field effect is too tiny to change the structure formation.[4] However, we shall not use the fitting to Equation (22) in this work, mainly for two reasons: first, the dark matter density profile is in general difficult to measure directly or precisely, while in contrast the circular velocities V_c of the stars rotating about the halo center are easier to measure; second, V_c as a function of radius R is more closely related to $\sqrt{\kappa}\delta\varphi(R)$, which will become clear later. As a result, we shall use fittings to V_c from here on.

Assuming Equation (22) as the density profile and sphericity of halos, we derive V_c easily as

$$V_c^2(R) = \frac{GM(R)}{R} = 4\pi G\beta\rho_c R_s^3 \left[\frac{1}{R}\ln\left(1+\frac{R}{R_s}\right) - \frac{1}{R_s+R}\right], \quad (23)$$

where $M(R)$ is the mass enclosed in radius R, and again this is parameterized by β and R_s. From a simulation point of view, it is straightforward to measure $M(R)$ and then fit β and R_s; from an observational viewpoint, it is easy to measure $V_c(R)$, which could again be used to fit β and R_s.

To show how good the fittings could be, we pick out nine halos with different masses and sizes from our simulation box, fit the corresponding β and R_s using the measured $M(R)$, and plot these in Figure 5. As can be seen there, the fitting results (solid curves) agree with the simulation results (crosses) quite well (in particular for the halo with $M = 3.895 \times 10^{13}\, M_{\odot}$).

To see how this could be related to $\sqrt{\kappa}\varphi$, we remember that in the above we have shown that $a\sqrt{\kappa}\varphi = 4\zeta\Phi$, and so all we need to do is to find an expression for $\Phi(R)$. For this, we use the fact that the potential inside a spherical halo is given as

$$\Phi(R) = \int_0^R \frac{GM(r)}{r^2} dr + C \quad (24)$$

in which $GM(r)/r^2$ is the gravitational force and C is a constant to be fixed using the fact that $\Phi(R = \infty) = \Phi_{\infty}$, where Φ_{∞} is the value of the potential far from the halo.

Using the formula for $GM(r)/r^2$ given in Equation (23), it is not difficult to find that

$$\int_0^R \frac{GM(r)}{r^2} dr = 4\pi G\beta\rho_c R_s^3 \left[\frac{1}{R_s} - \frac{\ln\left(1+\frac{R}{R_s}\right)}{R}\right]$$

[4] Indeed the NFW profile is quite robust, and even the scalar field does influence the structure formation significantly it is often still preserved. See examples for the coupled quintessence (Li & Barrow 2011), ReBEL (Keselman et al. 2010), and extended quintessence (Li et al. 2011) models.

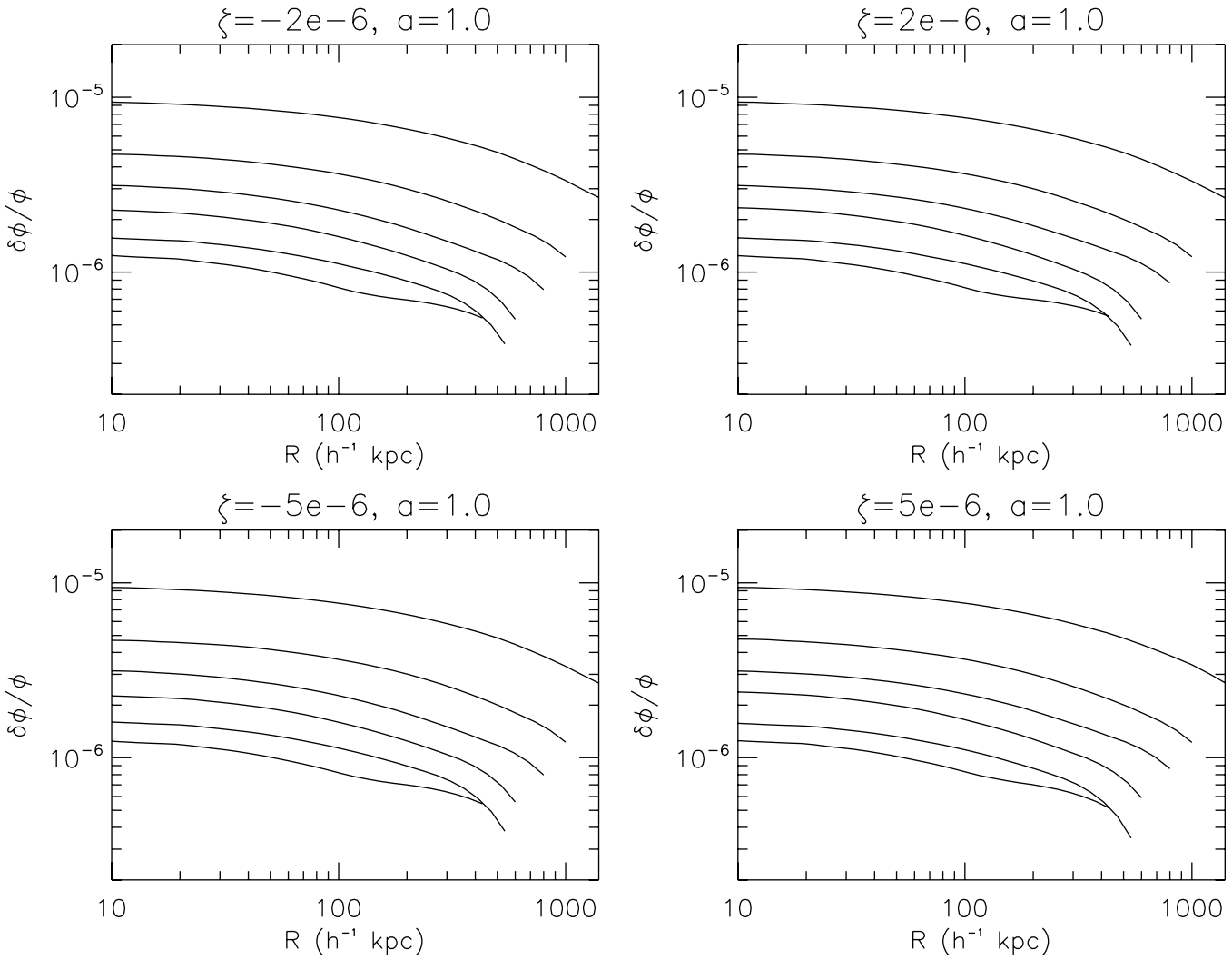

Figure 4. As Figure 3, except that this figure shows the profiles of $\delta\varphi/\varphi$ instead of $a\sqrt{\kappa}\delta\varphi$.

and so

$$C = \Phi_\infty - 4\pi G\beta\rho_c R_s^2. \tag{25}$$

Then it follows that

$$\Phi(R) = \Phi_\infty - 4\pi G\beta\rho_c \frac{R_s^3}{R} \ln\left(1 + \frac{R}{R_s}\right). \tag{26}$$

If the halo is isolated, then $\Phi_\infty = 0$ and we get

$$\Phi(R) = -4\pi G\beta\rho_c \frac{R_s^3}{R} \ln\left(1 + \frac{R}{R_s}\right). \tag{27}$$

However, in N-body simulations, we have a large number of dark matter halos and no halo is ideally isolated from the others. In such situations, Φ_∞ in Equation (26) should be replaced by

$$\Phi_* \equiv \Phi(R = R_* \gg R_{\rm vir}) \neq 0, \tag{28}$$

where R_* is some radius large compared with $R_{\rm vir}$ (the virialized halo radius) but small compared with inter-halo distances. Then we get

$$a\sqrt{\kappa}\delta\varphi(R) = 4\zeta\left[\Phi_* - 4\pi G\beta\rho_c \frac{R_s^3}{R} \ln\left(1 + \frac{R}{R_s}\right)\right]. \tag{29}$$

As an example to show how well Equation (29) works, we show in Figure 6 the results of $a\sqrt{\kappa}\delta\varphi(R)$ for the same halos used to fit β and R_s in Figure 5. Here, the crosses represent the values of $a\sqrt{\kappa}\delta\varphi$ measured from the N-body simulations and the curves represent our analytical approximations, in which the solid curve is obtained by setting $\Phi_* = \Phi_\infty = 0$, while the dashed curve is from tuning Φ_* appropriately. Obviously in most cases, there is a (nearly) constant shift of the approximation with respect to the numerical results, which accounts for Φ_* being non-zero.

Note that Equation (29) captures the shapes for $a\sqrt{\kappa}\delta\varphi$ in various halos, but there is still one free parameter, Φ_*, to be tuned to match the numerical results. This parameter summarizes our lack of knowledge about the environment in which the considered halo resides. As a result, formula (29) is most suitable for application in isolated halos, while for residential halos some extra work remains to be done to make it accurate.

Alternatively, one could also consider Equation (29) as a three-parameter parameterization of $a\sqrt{\kappa}\delta\varphi$, for which the three parameters β, R_s, and Φ_* could be fitted using the results from N-body simulations. Given all the above results, we expect that this could produce some nice fitting curves too, but we do not expand on this point here.

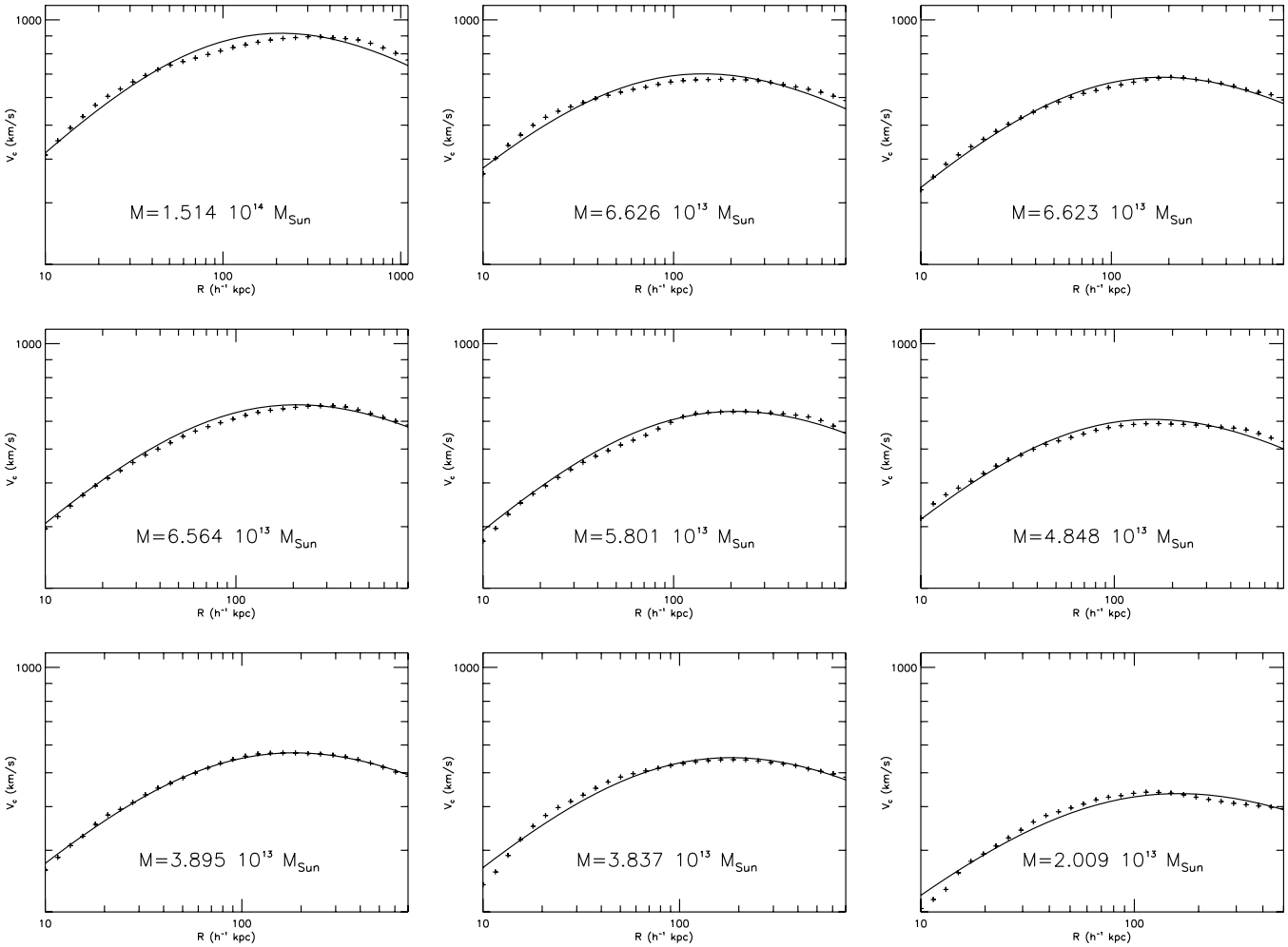

Figure 5. Fitting curves for the circular velocity, V_c, in the halo using the parameterization Equation (23). We show the results for nine halos selected from the 80 most massive ones in the simulation box, and their masses are given near the bottom of the each panel (the mass is decreasing from the upper left corner to the lower right corner). Solid curves are the fitting formulae while crosses are the N-body simulation results. All results are at the output time $a = 1.0$; the horizontal axis is the distance from the halo center in unit of h^{-1} kpc and vertical axis denotes V_c, in unit of km s^{-1}. Note that only the model with $\zeta = -2 \times 10^{-6}$ is displayed for clarity but other models give similar results.

4. SUMMARY AND CONCLUSION

To summarize, in this paper we have studied the behavior of the BSBM varying-α model in the highly nonlinear regime of large-scale structure formation, with the aid of full N-body simulations that explicitly solve the scalar field that controls the temporal and spatial variations of α.

We have checked that, because of the weak coupling to matter and the lack of (nonlinear) potential, the scalar field is indeed very light everywhere and thus does not cluster significantly, i.e., the spatial fluctuation of φ is tiny. Because of this property, we have been able to simplify the field equations, which in turn suggest that the scalar-field perturbation $\delta\varphi$ is proportional to the gravitational potential Φ (cf. Equation (19)). The numerical simulations then conform that such a simplification is justified to high precision.

We then concentrate on the profiles of the scalar field inside virialized halos, which galaxies (and observers) are supposed to reside in. Figures 3 and 4 display the averaged profiles of $a\sqrt{\kappa}\delta\varphi$ in the most massive halos from our simulation box, and they show that $a\sqrt{\kappa}\delta\varphi$ decreases as one goes from the halo center outward. In addition, the heavier the halo is, the deeper the gravitational potential will be and, as a result of Equation (19), the larger $a\sqrt{\kappa}|\delta\varphi|$ is. Interestingly, although $\delta\varphi$ does depends on the value of the BSBM parameter ζ, the quantity $\delta\varphi/\varphi$ is essentially independent of it (i.e., the same for BSBM models with different ζ from our parameter space of interest).

Thanks to the smallness of the scalar-field coupling, the background expansion rate and the source to the Poisson equation are essentially unaffected by the scalar field, while at the same time the fifth force is much weaker than ($\sim\zeta^2$ times) gravity so that its effect is also negligible. As a result, the structure formation itself is indistinguishable from that in pure ΛCDM model. In particular, the halo density profiles are very well described by the NFW fitting formula. Furthermore, the circular velocities V_c inside halos from the simulations are also well fitted using the analytical formula for V_c derived assuming NFW profiles (cf. Figure 5).

As another check of the fact that the scalar-field perturbation $\delta\varphi$ is proportional to the gravitational potential Φ (cf. Equation (19)), we have derived an analytical expression for $a\sqrt{\kappa}\delta\varphi$ again by assuming NFW halo density profiles (cf. Equation (29)). We adopt the NFW parameters fitted using the circular velocities measured from simulation outputs in Equation (29) and make predictions for $a\sqrt{\kappa}\delta\varphi$ in different halos. As shown in Figure 6, the predictions agree very well with

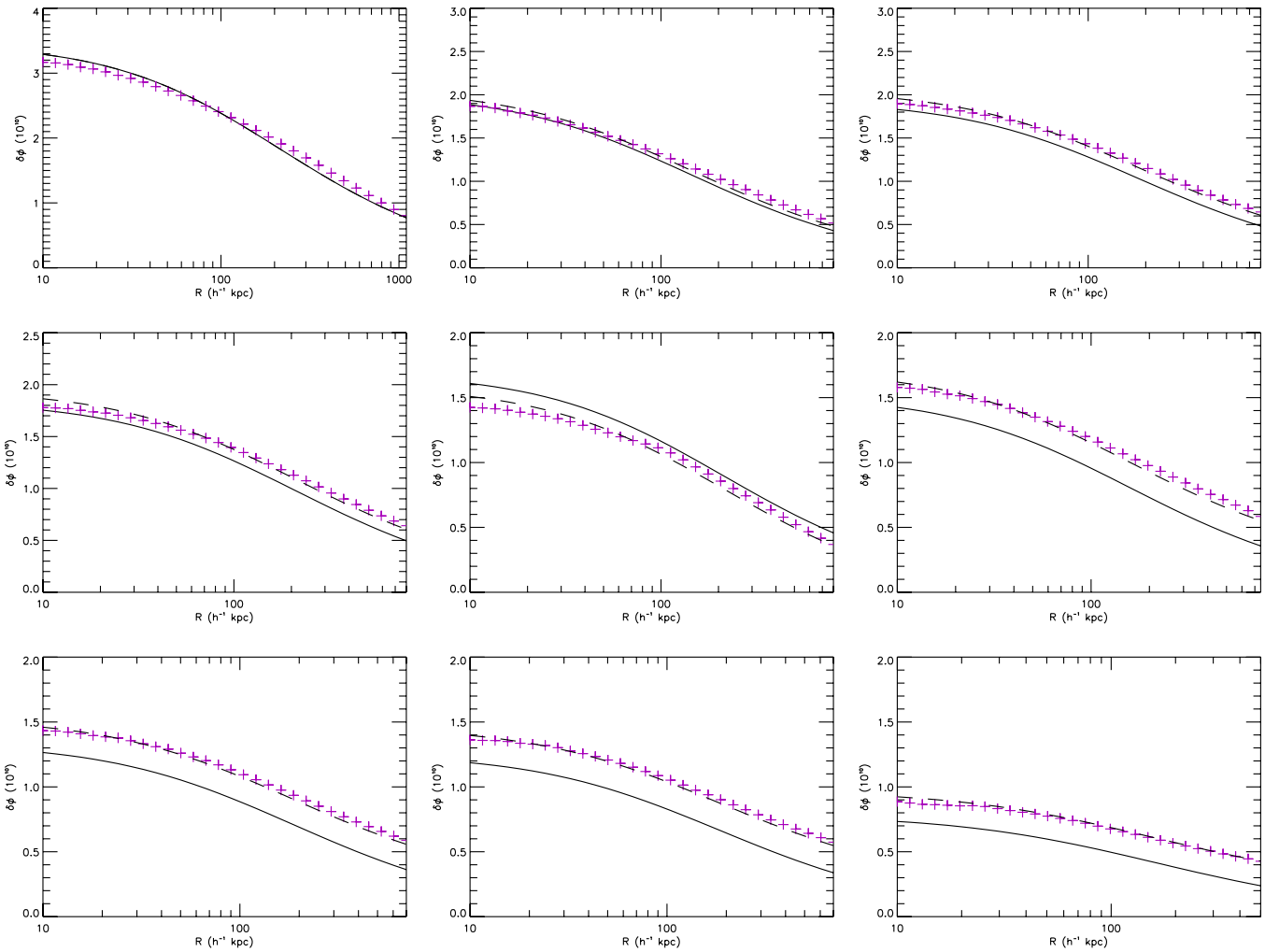

Figure 6. Analytical approximation compared with the numerical simulation results for the profile of $a\sqrt{\kappa}\delta\varphi$ in the same nine halos as in Figure 5. Purple crosses are the numerical results, the solid curve represents the analytical approximation Equation (29) with $\Phi_* = \Phi_\infty = 0$, and the dashed curve denotes Equation (29) with some tuned value of Φ_*. The parameters β and R_s are the best-fit values in Figure 5. All results are at the output time when $a = 1.0$; the horizontal axis is the distance from the halo center, in units of h^{-1} kpc and the vertical axis denotes $a\sqrt{\kappa}\delta\varphi$, in units of 10^{-10}. Note that only the model with $\zeta = -2 \times 10^{-6}$ is displayed for clarity but other models give similar results.

(A color version of this figure is available in the online journal.)

the numerical results for $a\sqrt{\kappa}\delta\varphi$, if we take into account the fact that halos are generally not isolated but living in potential wells produced by other halos.

Our results suggest that for simple coupled scalar-field models such as BSBM (and the one studied in Li & Barrow 2011), the properties of the scalar-field perturbation could be studied without solving the scalar-field equation of motion explicitly (which is time consuming). We could either extract them from, say, the halo density profiles (using our Equation (29)) of ΛCDM *N*-body simulations, or from the data on the galaxy rotation curves (using Equations (23) and (29)) from observations. In the latter case, it is interesting that two seemingly uncorrelated things could be studied together and only once.

Let us stress that the above nice properties are only present because of the smallness of the fluctuation in the scalar field, which is in turn due to the lack of significant nonlinearity in its equation of motion. If the scalar field is a chameleon, then its spatial fluctuation could be strong (Li & Zhao 2009, 2010; Zhao et al. 2010) and it then becomes impossible to obtain a simple analytical formula for $a\sqrt{\kappa}\delta\varphi$, such as Equation (29). *N*-body simulations will be the only tool to study such models, which we hope to investigate in the future.

The work described in this paper has been performed on TITAN, the computing facilities at the University of Oslo in Norway, utilizing a modified version of the MLAPM code (Knebe et al. 2001). Postprocessing is done on COSMOS, UK's National Cosmology Supercomputer, and the halo properties are obtained using a modified version of MHF (Knebe & Gibson 2004). We thank George Efstathiou for encouragement which helps bring this work to reality. B.L. is supported by the Research Fellowship at Queens' College, Cambridge, and the Science and Technology Facility Council (STFC) of the United Kingdom. D.F.M. thanks the Research Council of Norway FRINAT grant 197251/V30 and the Abel extraordinary chair UCM-EEA-ABEL-03-2010. D.F.M. is also partially supported by the projects CERN/FP/109381/2009 and PTDC/FIS/102742/2008.

REFERENCES

Barrow, J. D. 2002, The Constants of Nature (London: Jonathan Cape)
Barrow, J. D. 2005, Phil. Trans. R. Soc. A, 363, 2139
Barrow, J. D., Magueijo, J., & Sandvik, H. B. 2002a, Phys. Rev. D, 66, 043515
Barrow, J. D., & Mota, D. F. 2003, Class. Quantum Gravity, 20, 2045
Barrow, J. D., Sandvik, H. B., & Magueijo, J. 2002b, Phys. Rev. D, 65, 063504

Bekenstein, J. D. 1982, Phys. Rev. D, 25, 1527
Chand, H., Srianand, R., Petitjean, P., & Aracil, B. 2004, A&A, 417, 853
Clifton, T., Mota, D. F., & Barrow, J. D. 2005, MNRAS, 358, 601
Griest, K., Whitmore, J. B., Wolfe, A. M., Prochaska, J. X., Howk, J. C., & Marcy, G. W. 2010, ApJ, 708, 158
Jacobson, T. 1999, Phys. Rev. Lett., 83, 2699
Keselman, J. A., Nusser, A., & Peebles, P. J. E. 2010, Phys. Rev. D, 81, 063521
Knebe, A., & Gibson, B. K. 2004, MNRAS, 347, 1055
Knebe, A., Green, A., & Binney, J. 2001, MNRAS, 325, 845
Levshakov, S. A., Lapinov, A. V., Henkel, C., Molaro, P., Reimers, D., Kozlov, M. G., & Agafonova, I. I. 2010a, A&A, 524, 32
Levshakov, S. A., Molaro, P., Lapinov, A. V., Reimers, D., Henkel, C., & Sakai, T. 2010b, A&A, 512, 44
Levshakov, S. A., Molaro, P., & Reimers, D. 2010c, A&A, 516, 113
Li, B., & Barrow, J. D. 2011, Phys. Rev. D, in press (arXiv:1005.4231)
Li, B., Mota, D. F., & Barrow, J. D. 2011, ApJ, 728, 109
Li, B., & Zhao, H. 2009, Phys. Rev. D, 80, 044027
Li, B., & Zhao, H. 2010, Phys. Rev. D, 81, 104047
Magueijo, J., Barrow, J. D., & Sandvik, H. 2002, Phys. Lett. B, 549, 284
Mota, D. F., & Barrow, J. D. 2004a, MNRAS, 349, 291
Mota, D. F., & Barrow, J. D. 2004b, Phys. Lett. B, 581, 141
Murphy, M. T., Webb, J. K., & Flambaum, V. V. 2007, Phys. Rev. Lett., 99, 239001
Murphy, M. T., Webb, J. K., & Flambaum, V. V. 2008, MNRAS, 384, 1053
Navarro, J. F., Frenk, C. S., & White, S. D. M. 1996, ApJ, 462, 563
Olive, K. A., & Pospelov, M. 2008, Phys. Rev. D, 77, 043524
Olive, K. A., & Qian, Y.-Z. 2004, Phys. Today, 57, 40
Sandvik, H. B., Barrow, J. D., & Magueijo, J. 2002, Phys. Rev. Lett., 88, 031302
Shaw, D. J., & Barrow, J. D. 2006a, Phys. Lett. B, 639, 596
Shaw, D. J., & Barrow, J. D. 2006b, Phys. Rev. D, 73, 123505
Shaw, D. J., & Barrow, J. D. 2006c, Phys. Rev. D, 73, 123506
Srianand, R., Chand, H., Petitjean, P., & Aracil, B. 2004, Phys. Rev. Lett., 92, 121302
Srianand, R., Chand, H., Petitjean, P., & Aracil, B. 2008, Phys. Rev. Lett., 100, 029902
Uzan, J.-P. 2003, Rev. Mod. Phys., 75, 403
Uzan, J.-P. 2010, arXiv:1009.5514
Webb, J. K., Flambaum, V. V., Churchill, C. W., Drinkwater, M. J., & Barrow, J. D. 1999, Phys. Rev. Lett., 82, 884
Webb, J. K., King, J. A., Murphy, M. T., Flambaum, V. V., Carswell, R. F., & Bainbridge, M. B. 2010, arXiv:1008.3907
Webb, J. K., Murphy, M. T., Flambaum, V. V., Dzuba, V. A., Barrow, J. D., Churchill, C. W., Prochaska, J. X., & Wolfe, A. M. 2001, Phys. Rev. Lett., 87, 091301
Wetterich, C. 2003, J. Cosmol. Astropart. Phys., JCAP10(2003)002
Whitmore, J. B., Murphy, M. T., & Griest, K. 2010, ApJ, 723, 89
Zhao, H., Maccio, A. V., Li, B., Hoekstra, H., & Feix, M. 2010, ApJ, 712, L179